JTTEE5 13:390-395
DOI: 10.1361/10599630420425
1059-9630/$19.00 © ASM International

Peer Reviewed

Strain Analysis of Plasma Sprayed Thermal Barrier Coatings Under Mechanical Stress

T. Wakui, J. Malzbender, and R.W. Steinbrech

(Submitted October 1, 2003; in revised form December 23, 2003)

The stiffness of air plasma sprayed (APS) thermal barrier coatings (TBCs) was determined from bending experiments combining strain analysis on a microstructural level with macroscopic mechanical parameters. Tests were performed with freestanding and attached TBCs, the latter either loaded in tension or in compression. Relationships are derived, which describe the TBC stiffness in a multilayer composite (attached TBC) and for a bimodular material that possess a lower stiffness in tension than in compression (stand-alone TBC). The increase of in-plane stiffness with increasing compressive stress emphasizes the importance of the spraying defects for the elastic response of the coating.

Keywords bending test, stiffness, strain, thermal barrier coating (TBC)

1. Introduction

Ceramic thermal barrier coatings (TBCs) are increasingly used on high-temperature-exposed components of advanced gas turbines to extend the operational temperature and/or to decrease internal cooling, which in both cases increases the efficiency of the turbine.[1,2] Typically, the components consist of a three-layer composite. The single-crystal Ni-superalloy substrate is corrosion protected by a metallic layer that also provides the bond coat (BC) for the insulating porous ceramic top coat. The standard TBCs are either atmospheric plasma sprayed (APS) or physically electron beam-vapor deposited (EB-PVD) yttria-stabilized zirconias. Depending on the coating process different microstructures develop, i.e., spraying lamellae parallel to the BC in the case of APS or columnar grains perpendicular to the BC in the case of EB-PVD.

The mismatch in thermal expansion coefficients among substrate, BC, and TBC results in residual stresses which, along with the brittleness of ceramic coatings and the formation of a thermally grown oxide (TGO) between BC and TBC, often lead to delamination or segmentation cracks, which ultimately cause spallation.[3-7] The stiffness of the TBCs is considered as a key parameter to quantify the stress situation and the brittle failure behavior of the thermal barrier system.

Frequently a relatively low macroscopic stiffness is reported for TBCs and attributed to pores and the large number of microcracks.[8] The low stiffness leads to low residual stresses in the TBC and in consequence to a relatively high thermomechanical stability. The microstructure and thus the elastic properties, however, may undergo changes during long-term exposure at high temperature. Formation of the TGO, sintering processes[8] and crack healing within the TBC splats[9,10] are assumed to change the local residual stress situation and to lead to an increase in TBC stiffness, respectively. Hence, TBC failure and fatigue of the thermal barrier composite become more likely by thermal exposure of the coating. Measurement of the TBC stiffness provides a tool to assess the reliability of the thermal barrier system.[8]

The stiffness of TBCs has been measured using different methods, e.g., ultrasonic techniques,[11] mechanical bending,[8,12] and indentation tests.[8,10,13] In particular, the indentation method is widely used to determine the mechanical properties of coatings.[14] The microprobing capability is an advantage of indentation testing compared with macroscopic bending experiments. However, typically the obtained stiffness reveals a strong dependence on the indentation load.[13] Discrete boundaries and microstructural defects are involved in the deformation process accompanying the impression and lead to significantly lower values of the stiffness compared with the properties of bulk YSZ. In addition, a large scatter of the measured data is obtained. Moreover, the mechanical properties can differ due to the microstructural anisotropy of the coatings.[15]

Lower stiffness values are typically obtained from averaging global measurements of TBCs as realized in bending tests.[8] These tests reveal, compared with indentation, the elastic response of a much larger volume of coating. Since the global stiffness results appear to be less affected by experimental and local material parameters, it seems reasonable to study the influence of stress on stiffness in a global approach.

In the present paper, bending techniques with in situ observation of the TBC surface are used to characterize the global elastic properties of attached and stand-alone APS TBCs. The stiffness is determined by combining strain analysis from microscopic observations with the mechanical stress data of the bending tests. In particular, the influence of stress and strain on stiffness is elaborated.

2. Experimental

ZrO_2-based (7-8 wt.% Y_2O_3) thermal barrier coatings (300 μm) were deposited with a Metco-Triplex I plasma gun (Sulzer Metco, Winterthur, Switzerland) on larger plates of low-pressure plasma sprayed bond coat with underlying Ni-superalloy substrate. To prepare stand-alone TBC specimens thick YSZ coating (~2 mm) was also sprayed directly on a steel substrate. All coatings were carried out at the Institute for Materials and Processes in Energy Systems, IWV 1, Research Center Jülich, Ger-

T. Wakui, J. Malzbender, and **R.W. Steinbrech,** Institute for Materials and Processes in Energy Systems, Forschungszentrum Jülich, D-52428 Jülich, Germany. Contact e-mail: j.malzbender@fz-juelich.de.

Table 1 Elastic Moduli E_i, Thermal Expansion Coefficients α_i and Thickness of the Layers t_i in the Thermal Barrier Specimens

	t_i, µm	E_i, GPa	α_i, 10^{-6} K^{-1} (20-800 °C)
Ni-superalloy substrate	380-910	122	11.5-15.6
NiCoCrAlY bond coat	140	140	10.3-16.0
TBC	320-2000	…	9.7-10.3

many. During the air plasma spraying, the substrates were cooled with compressed air resulting in deposition temperatures between 200 and 250 °C. After cooling to room temperature, the TBC surfaces of the specimens were polished with diamond paste to facilitate microscopic observation (final polishing step 1 µm). From the specimens with thick TBC the substrate was removed via chemical etching with hydrochloric acid.

The bending experiments were carried out with small devices mounted on the stages of an optical and a scanning electron microscope. The determination of the strain was based on a comparison of in situ recorded micrographs using the commercial software UNIDAC (Universal Deformation Analysis by Means of Correlation, Chemnitzer Werkstoffmechanik GmbH, Chemnitz, Germany), which permits a strain analysis via gray-scale image contrast.[16]

The stiffness was calculated assuming a linear-elastic relationship between stress and strain. The actual relationships applied for the stiffness determination are outlined in the following section. Special care was taken to consider the multilayer stress situation and the influence of thermal mismatch as given in a thermal barrier system. The elastic moduli E_i, thermal expansion coefficient α_I, and thickness of the layers t_i, which had to be known to determine the stress and strain in the TBC, are given in Table 1.

3. TBC Strain in Bending

3.1. Multilayer Composite-Attached TBC

The strain/deflection correlations given in the following describe the behavior of coatings with different stiffness in tension and compression (e.g., plasma sprayed thermal barrier coatings). Typically, stiffness is treated as an average value that can be determined, for example, mechanically in bending tests as a secant or tangential value from the stress-strain or load-deflection curve. However, performing a set of measurements with loading to different strains also permits a determination of the respective average stiffness as a function of applied strain. A determination of the stiffness as a function of the absolute strain requires a consideration of the residual stress. The stiffness at zero strain can be calculated via extrapolation.

In the case of the attached TBCs, the specimens are analyzed by applying a bending moment perpendicular to the interface between the layers, which corresponds to bending parallel to the spraying direction. Figure 1 outlines the geometrical situation for a three-layer thermal barrier composite. The elastic theory of multilayered composites yields for bending perpendicular to the interface between the layers a flexural rigidity of[17]

$$(EI)^* = \frac{1}{3} w \sum_{i=1}^{n} E_i \left[\left(\sum_{j=1}^{i} t_j - t_{na} \right)^3 + \left(t_{na} - \sum_{j=1}^{i-1} t_j \right)^3 \right] \quad \text{(Eq 1)}$$

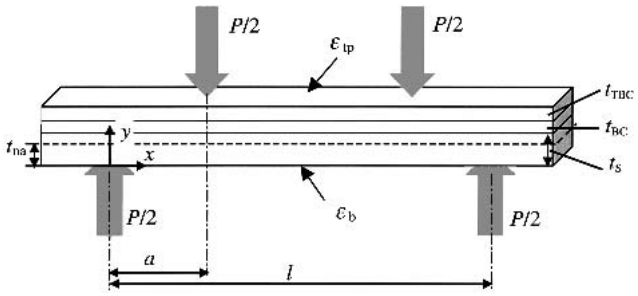

Fig. 1 Layer geometry of thermal barrier composite in four-point bending test

where w is the width of the beam and the neutral axis (Fig. 1) is[17]

$$t_{na} = w \sum_{i=1}^{n} E_i t_i \left(2 \sum_{j=1}^{i=1} t_j + t_i \right) \Big/ \left(2 \sum_{i=1}^{n} E_i w_i t_i \right) \quad \text{(Eq 2)}$$

The strain can be measured on the free surfaces of the top and the bottom layer (Fig. 1). In each case the strain $\Delta\varepsilon$ is related to the flexural rigidity of the multilayered composite beam EI^*. The tensile strain on the free surface of the top layer (Fig. 1) is[17]

$$\Delta\varepsilon_{tp} = \frac{\Delta M}{(EI)^*} \left(\sum_{1}^{n} t_i - t_{na} \right) \quad \text{(Eq 3)}$$

and the compressive strain on the free surface of the bottom layer (Fig. 1) becomes

$$\Delta\varepsilon_b = \frac{\Delta M}{(EI)^*} (t_{na}) \quad \text{(Eq 4)}$$

The applied moment is in the case of four-point bending $\Delta M = \Delta P a/2$. In the case that the specimen is thin compared with the distance between the loading spans, the flexural rigidity of the composite beam is related with the load-deflection behavior as[17]

$$(EI)^* = f(a) \frac{\Delta P}{\Delta d} \quad \text{(Eq 5)}$$

where the geometry-function $f(a)$ in a four-point bending experiment becomes $f(a) = a(3lx - 3x^2 - a^2)/12$ (Fig. 1). Here l is the loading span, a the distance between inner and outer loading pins, and x the position with respect to the outer loading pin at which the deflection d is measured.

Equation 5 can be combined with either Eq 3 or 4 to determine the stiffness of the TBC as a function of the applied tensile or compressive stress. Alternatively, as has been done here, the stiffness as a function of the applied tensile or compressive stress can be determined directly from Eq 3 or 4, respectively. In this case the relationship for the flexural rigidity, Eq 1 has to be solved for the unknown stiffness of the TBC. Since the solution is straightforward but rather lengthy, an explicit equation is not given here but can conveniently be obtained with suitable math programs.

3.2. Residual Stress in the TBC

Since the stiffness is supposed to be a function of the applied stress, the bending stress for the layer n can be estimated using Eq 3. However, in the multilayered composites frequently residual stresses due to thermal mismatch also exist. Considering the residual stress $\sigma_{res,y}$ at the position y within the layer i, one obtains the more general relationship:[17]

$$\sigma_{i,y} = \frac{E_i \Delta M}{(EI)^*}(y) + \sigma_{res,i,y} \quad \text{(Eq 6)}$$

Values of the residual stress in the TBC can be obtained independently of the bending tests, e.g., by multilayer curvature experiments.[18]

3.3. Stand-Alone TBCs

Stand-alone TBCs need a special treatment since they exhibit a steady transition (gradient) from tensile to compressive stress upon loading in a bending test. Due to the stress dependency of the stiffness only a trivial solution can be obtained applying the same procedure as before to a stand-alone TBC. As a simplified extension to the mechanical analysis presented above, two isotropic TBC materials with different stress-dependent stiffness are considered. The thickness of the specimen volume under compression is $t_c = t_{na}$. The subscript c refers in the following to the specific volume under compression and subscript t to the volume under tension. Equation 2 leads for the average stiffness at the applied strain $\Delta\varepsilon = q$ to[17]

$$\overline{E_{t,q}}\, t_{t,q}^2 = \overline{E_{c,q}}\, t_{c,q}^2 \quad \text{(Eq 7)}$$

Since $t_c = t_{na}$, Eq 1 can be simplified to obtain:

$$(EI)^* = \frac{w}{3}\left(\overline{E_{c,q}}\, t_{c,q}^3 + \overline{E_{t,q}}\, t_{t,q}^3\right) \quad \text{(Eq 8)}$$

Strain measurements on the side face provide the position of the neutral axis. Using Eq 7 and 8, the average stiffness of the portion under tension then becomes:

$$\overline{E_{t,q}} = \frac{3\Delta M}{\Delta\varepsilon\, wt(t - t_{na})} \quad \text{(Eq 9)}$$

The average stiffness of the portion under compression can be determined from[17]

$$\overline{E_{c,q}} = \frac{3\Delta M\,(1 - t_{na}/t)}{\Delta\varepsilon\, w(t_{na})^2} \quad \text{(Eq 10)}$$

The stiffness values in the following results section are obtained as a secant modulus with the analytical approaches outlined above. In the case of attached TBCs the strain was determined by an analysis of images taken from the side face of the specimen (Fig. 2, Eq 3-5). For the freestanding TBCs the calculation of the strain was performed on the basis of images taken from the surface and the side face (Fig. 2, Eq 9 and 10).

4. Results and Discussion

The stiffness response of the TBC to mechanical loading is subsequently addressed under two aspects. First the local nature of deformation and straining is demonstrated. Thereafter, in an averaging approach, the stress dependence of the global stiffness is quantified and compared with results from literature.

4.1. Local Strain Aspect

A SEM micrograph of an arbitrary location of the tensile surface of a stand-alone TBC specimen is shown in Fig. 3. In addition, the inlet displays the displacement vectors obtained by gray-scale analysis comparing the initial and a progressed stage of bending. A pronounced change in displacement along the cracklike defect can be seen. The inhomogeneous microstructure of the APS TBC results in a variation of the displacement for different local areas. This is illustrated in Fig. 4, where the stiffness was determined for six different areas with different local microstructure. The values obtained as the ratio of applied stress divided by local strain vary from 1.2-30.6 GPa. An analysis covering the total area of the micrograph results in an average value of ~5 GPa. Obviously the high compliance of larger defects severely influences the mechanically measured global tensile stiffness of the TBC. Likewise, under compression a higher stiffness can be expected when the crack surfaces are forced into physical contact.

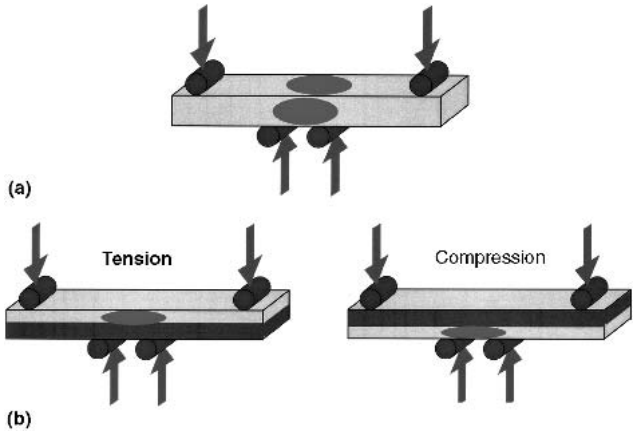

Fig. 2 Strain determination of TBCs in bending tests by comparison of surface images from in situ microscopic observation. Bending tests were carried out with **(a)** stand-alone and **(b)** attached TBCs under tension and compression.

Note that, as a consequence, a load-dependent shift of the neutral axis toward the compressive specimen side also has to be considered when bending tests are carried out with separated stand-alone TBCs.

A second aspect of the defect-governed deformation behavior is the localization of straining in the TBC. Contour plots of the strain $\Delta\varepsilon_x$ in the cross section of an attached TBC obtained during stepwise application of tensile loads from 38-248 N are displayed in Fig. 5. The section shown for a fixed position in each strain map covers the area between TBC surface (top) and interface to the bond coat (bottom). The contour maps reveal different stages of the localized formation of segmentation cracks.

Similarly, contour plots of the strain $\Delta\varepsilon_y$ in the cross section of an attached TBC obtained during stepwise application of compressive loads from 28-148 N are displayed in Fig. 6. The cross section now has the TBC surface at the bottom and the interface at the top. The opening of a larger delamination crack near the interface to the bond coat is recognized.

In terms of a minimum strain required for opening activity of larger cracks in segmentation and delamination orientation, an average value in the order of ~0.2% can be deduced if higher resolution of the strain maps is chosen.

The micrograph in Fig. 4 and the contour plots in Fig. 5 and 6 illustrate how the inhomogeneous microstructure affects the local strain behavior of a TBC. It is emphasized that this heterogeneity aspect should receive more attention in future stiffness characterization studies.

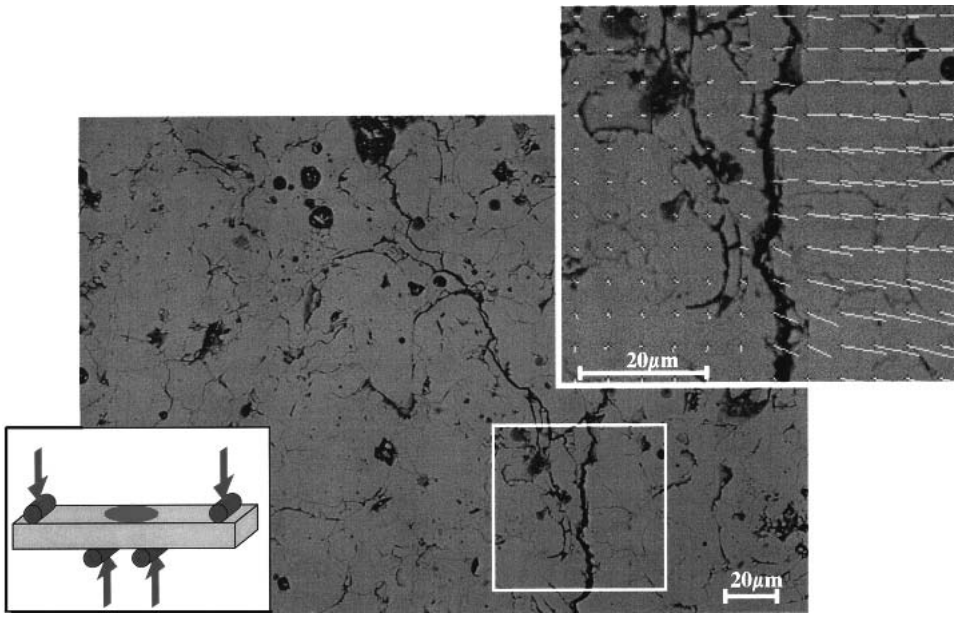

Fig. 3 Scanning electron micrograph of tensile surface (stand-alone TBC) in bending test. Displacement field around crack-shaped defect (inlet) reflects changes upon loading as obtained by gray-scale analysis.

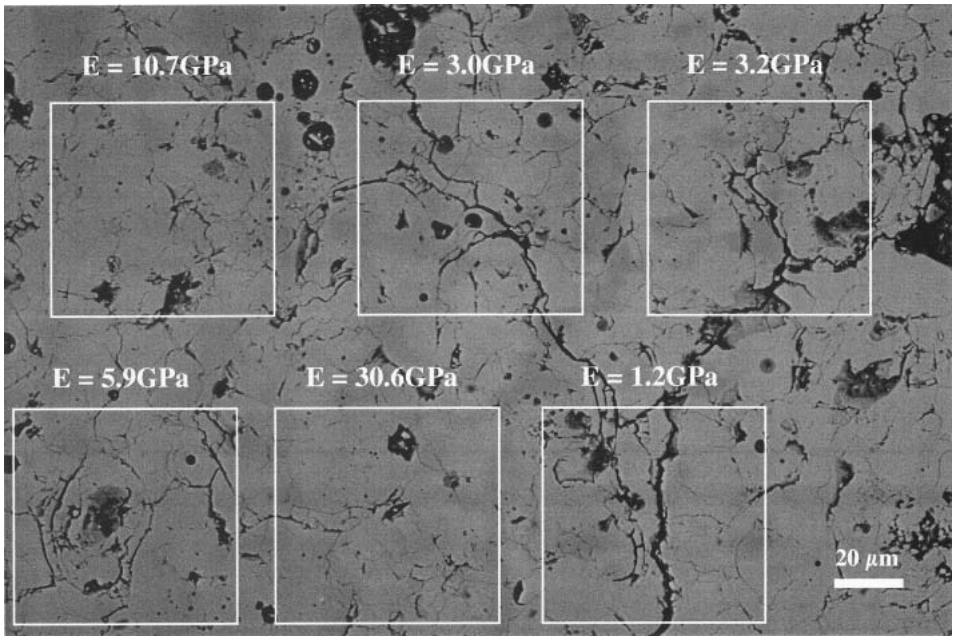

Fig. 4 Determination of average stiffness for six smaller areas in the micrograph of Fig. 3. Results illustrate the influence of microstructural defects on variation of stiffness in TBC.

4.2. Global Strain Aspect

To quantify the macroscopic stiffness response of the TBC to an applied stress, the total strain mapping areas of bending tests were considered. For simplification, only the average stiffness from such areas was taken as a measure of the global response to the applied stress. Of course, in a more complex approach the stiffness values must reflect the strain gradient in the bending experiments, too. The changes in stiffness as a function of the total stress are plotted in Fig. 7. Note that, for both tensile and compressive loading, the total stress comprises the applied and the residual stress contributions (Eq 6). For the attached TBC a residual stress of ~50 MPa was assumed.[18] The data for the attached TBC under compressive and tensile stress are complementary and agree well if extrapolated to zero applied stress. The stiffness of the TBC increases considerably with applied compressive stress from a stress-free value of ~15 GPa to ~40 GPa at a compressive stress of 300 MPa.

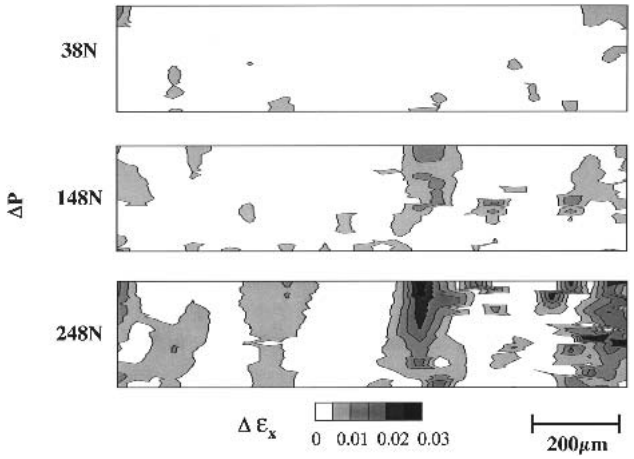

Fig. 5 Strain maps of attached TBC under tension. The analyzed TBC section is localized on side face of specimen. The section covers the area between free surface (top) and interface to BC (bottom). The contour plots show heterogeneous development of $\Delta\varepsilon_x$ strain as a function of increasing tensile load.

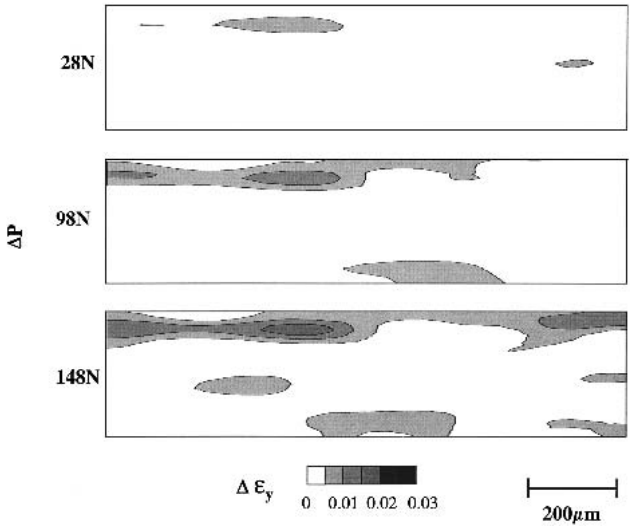

Fig. 6 Strain maps of attached TBC under compression. Side face view of TBC as in Fig. 5, but area shown with interface to BC at top and free surface at bottom. The contour plots represent development of localized $\Delta\varepsilon_y$ strain as a function of increasing in-plane compressive load.

Figure 7 also reveals a stiffness decrease with applied tensile stress. However, the measured tensile stress range is limited since stand-alone TBCs fracture at low stress levels of ~20-30 MPa,[19] and the formation of through-thickness segmentation cracks terminates the stiffness determination of attached TBCs. The data for the attached and stand-alone TBC agree reasonably well; the observed small deviations might also be related to differences in the local crack density.

The measured dependence of the stiffness on stress is compared in Fig. 8 with data reported in literature for APS[20] and EB-PVD[21,22] coatings. The results are restricted to the compressive stress regimen. For the APS TBC only a narrow range of stresses has been analyzed. There is good agreement for the

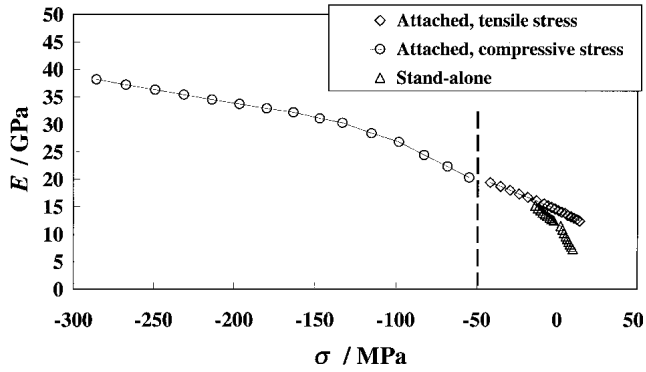

Fig. 7 Average stiffness of APS TBC as a function of the total stress σ_x (applied + residual). Shown are values for attached TBC under compressive and tensile stress together with data for the freestanding TBC. In the latter case, results for both stress states are obtained from single specimen measurements. For the attached TBC a residual stress of 50 MPa was assumed, as indicated by dashed vertical line.

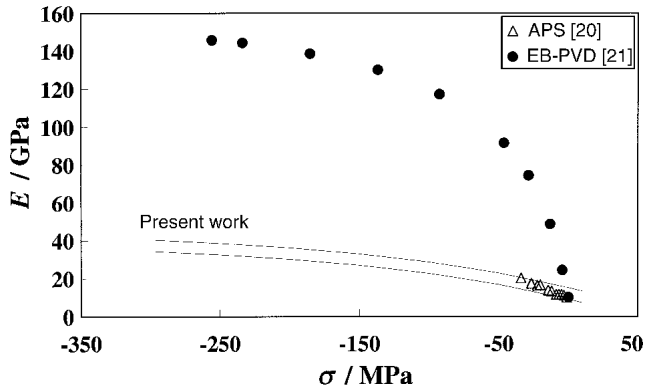

Fig. 8 Stiffness as a function of stress; comparison of data from Fig. 7 with results from literature for APS and EB-PVD coatings

secant modulus of the APS coatings in the common stress regimen, although residual stresses have not been considered. For large compressive stress, values close to the stiffness of the bulk material should be reached,[23] but the results of the current study do not support this theoretical assumption. In the bending tests, spallation occurred long before complete densification was achieved.

In comparison, the stiffness of the EB-PVD coating[21] shows a stronger dependence on stress, as might be expected from the narrow gaps between the columnar grains. Also, the stress at which the extrapolated stiffness approaches zero is lower (~5 MPa), being an indication of a lower modulus of rupture, as can be expected considering the weak interfaces between the columnar grains.

In comparing stiffness data obtained using different methods, it is usually not considered that different stress-strain conditions might be present in the TBC. Only residual stresses have to be taken into account to validate ultrasonic measurements. Indentation tests reflect the stiffness as a result of the TBC response between a minimum stress value, which is the residual stress, and a maximum value, which is the sum of the residual stresses from thermal mismatch and indentation. In bending tests of an

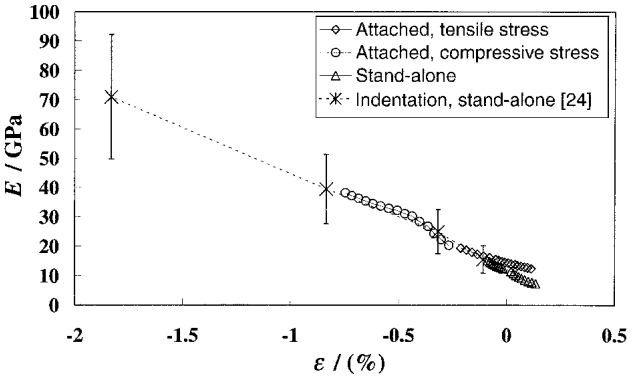

Fig. 9 Stiffness as a function of strain; comparison of the bending results with stiffness data obtained from spherical indentation experiments

attached TBC, the stiffness behavior varies as a function of the stress-strain state between interface and free surface. In bending tests of a stand-alone TBC, the tensile and compressive stresses have maximum values at the free surfaces and decrease toward the neutral axis of the specimen. Considering that the stiffness is a function of the stress-strain, it is not surprising that different methods can lead to different stiffness values. Since the TBCs show nonlinear stress-strain characteristics, the authors suggest plotting the stiffness as a function of strain.

To demonstrate the advantage of such a presentation, the data from the bending tests are compared with the stiffness values obtained for the same TBC using a spherical indenter.[24] In Fig. 9, the average value of indentation stiffness results from attached and stand-alone TBCs is related to half of the maximum applied strain. With these simplifying assumptions good agreement between indentation and bending results is obtained.

5. Conclusions

The stiffness of stand-alone and attached APS TBCs was derived on the basis of an elastic multilayer approach. The experimental strain values were obtained from image contrast analysis of scanning electron and optical micrographs. The results highlight the effect of inhomogeneous microstructure on elastic behavior and the pronounced dependency of the stiffness on the applied and residual stress-strain.

Acknowledgments

The authors would like to thank Robert Vassen for preparing the TBC material and E. Wessel for contributing to the scanning electron microscopy studies. Lorenz Singheiser provided continuous, encouraging support of the work, which is gratefully acknowledged.

References

1. H.W. Grünling and W. Mannsmann: "Plasma-Sprayed Thermal Barrier Coatings for Industrial Gas-Turbines—Morphology, Processing and Properties," *J. Phys. (Paris) IV,* 1993, *3*(C7), pp. 902-12.
2. J.T. DeMasi-Marcin and D.K. Gupta: "Protective Coatings in the Gas-Turbine Engine," *Surf. Coat. Technol.,* 1994, *68,* pp. 1-9.
3. D.B. Marshall and A.G. Evans: "Measurement of Adherence of Residually Stressed Thin-Films by Indentation: 1. Mechanics of Interface Delamination," *J. Appl. Phys.,* 1984, *56*(10), pp. 2632-38.
4. A.G. Evans and J.W. Hutchinson: "On the Mechanics of Delamination and Spalling in Compressed Films," *Int. J. Solids Struct.,* 1984, *20*(5), pp. 455-66.
5. A.K. Sinha, H.J. Levinstein, and T.E. Smith: "Thermal-Stresses and Cracking Resistance of Dielectric Films (SiN, Si_3N_4, and SiO_2) on Si Substrates," *J. Appl. Phys.,* 1978, *49*(4), pp. 2423-26.
6. S. Kuroda and T.W. Clyne: "The Quenching Stress in Thermally Sprayed Coatings," *Thin Solid Films,* 1991, *200*(1), pp. 49-66.
7. T.W. Clyne and S.C. Gill: "Residual Stresses in Thermal Spray Coatings and Their Effects on Interfacial Adhesion: A Review of Recent Work," *J. Therm. Spray Technol.,* 1996, *5*(4), pp. 401-18.
8. J.A. Thompson and T.W. Clyne: "The Effect of Heat Treatment on the Stiffness of Zirconia Top Coats in Plasma-Sprayed TBCs," *Acta Mater.,* 2001, *49*(9), pp. 1565-75.
9. J. Ilavsky, G.G. Long, A.J. Allen, and C.C. Berndt: "Evolution of the Void Structure in Plasma Sprayed YSZ Deposits During Heating," *Mater. Sci. Eng.,* 1999, A*272,* pp. 215-21.
10. R.W. Steinbrech: "Thermomechanical Behavior of Plasma Sprayed Thermal Barrier Coatings," *Ceram. Eng. Sci. Proc.,* 2002, *23,* pp. 379-408.
11. J.I. Eldridge, G.N. Morscher, and S.R. Choi: "Quasistatic vs. Dynamic Modulus Measurements of Plasma Sprayed Thermal Barrier Coatings," *Ceram. Eng. Sci. Proc.,* 2002, *23,* pp. 371-80.
12. A. Kucuk, C.C. Berndt, U. Senturk, R.S. Lima, and C.R.C. Lima: "Influence of Plasma Spray Parameters on Mechanical Properties of Yttria Stabilized Zirconia Coatings: Four Point Bending Test," *Mater. Sci. Eng. A.,* 2000, *284,* pp. 29-40.
13. D. Basu, C. Funke, and R.W. Steinbrech: "Effect of Heat Treatment on Elastic Properties of Separated Thermal Barrier Coatings," *J. Mater. Res.,* 1999, *14*(12), pp. 4643-50.
14. J. Malzbender, J.M.J. den Toonder, A.R. Balkenende, and G. de With: "Measuring Mechanical Properties of Coatings: A Methodology Applied to Nano-Particle-Filled Sol-Gel Coatings on Glass," *Mater. Sci. Eng. R.,* 2002, *36*(2-3), pp. 47-103.
15. A. Wanner and E. Lutz: "Elastic Anisotropy of Plasma Sprayed, Free-Standing Ceramics," *J. Am. Ceram. Soc.,* 1997, *80*(8), pp. 2706-08.
16. E. Kieselstein, B. Seiler, M. Dost, and E. Than: "Characterization of Composites by Measuring the Optical Displacements via UNIDAC," *Technisches Messen,* 2002, *69*(10), pp. 412-17.
17. J. Malzbender and R.W. Steinbrech: "Mechanical Methods to Determine Layer Compliances within Multilayer Composites," *J. Mater. Res.,* 2003, *18*(6), pp. 1374-82.
18. G. Blandin: "Thermomechanical Behavior of Plasma Sprayed Thermal Barrier Composites," Doctoral Thesis, RWTH Aachen, Germany, 2001, pp. 43-46 (in German).
19. S.R. Choi, D. Zhu, and R.A. Miller: "Deformation and Strength Behavior of Plasma Sprayed ZrO2-8wt.% Y2O3 Thermal Barrier Coatings in Biaxial Flexure and Trans Thickness Tension," *Ceram. Sci. Eng. Proc.,* 2000, *21,* pp. 653-61.
20. V. Harok and K. Neufuss: "Elastic and Inelastic Effects in Compression in Plasma Sprayed Ceramic Coatings," *J. Thermal Spray Technol.,* 2001, *10*(1), pp. 126-32.
21. A.G. Evans, D.R. Mumm, J.W. Hutchinson, G.H. Meier, and F.S. Pettit: "Mechanism Controlling the Durability of Thermal Barrier Coatings," *Prog. Mater. Sci.,* 2001, *46,* pp. 505-53.
22. C.A. Johnson, J.A. Ruud, R. Bruce, and D. Wortmann: "Relationship Between Residual Stress, Microstructure and Mechanical Properties of Electron Beam-Physical Vapor Deposition Thermal Barrier Coatings," *Surf. Coat. Technol.,* 1998, *108-109,* pp. 80-85.
23. F. Kroupa and J. Doubsky: "Pressure Dependency of Young's Moduli of Thermal Spray Materials," *Scr. Mater.,* 1999, *40*(11), pp. 1249-54.
24. J. Malzbender and R.W. Steinbrech: "Determination of the Stress-Dependent Stiffness of Plasma Sprayed Thermal Barrier Coatings Using Depth Sensitive Indentation," *J. Mater. Res.,* 2003, *18*(8), pp. 1975-84.